Review

The Indian Summer Monsoon from a Speleothem $\delta^{18}O$ Perspective – a Review

Nikita Kaushal[1*], Sebastian F.M. Breitenbach[2], Franziska A. Lechleitner[3], Ashish Sinha[4], Vinod C. Tewari[5], Syed Masood Ahmad[6], Max Berkelhammer[7], Shraddha Band[8], Madhusudan Yadava[8], Rengaswamy Ramesh[9], Gideon M. Henderson[3]

[1] University of Oxford, Department of Earth Sciences, Oxford OX1 3AN, United Kingdom.
Now at: Asian School of the Environment, Nanyang Technological University; nkaushal@ntu.edu.sg

[2] Ruhr University Bochum, Institute for Geology, Mineralogy and Geophysics, Bochum 44801, Germany; sebastian.breitenbach@rub.de

[3] University of Oxford, Department of Earth Sciences, Oxford OX1 3AN, United Kingdom; franziska.lechleitner@ox.ac.uk; gideonh@earth.ox.ac.uk

[4] California State University, Dominguez Hills, Department of Earth Sciences, California 90747, United States of America; asinha@csudh.edu

[5] Sikkim University, Department of Geology, Sikkim 737102, India; vctewari@cus.ac.in

[6] Jamia Millia Islamia, Department of Geography, Faculty of Natural Sciences, New Delhi 110025, India; smasoodahmad@rediffmail.com

[7] University of Illinois, Department of Earth and Environmental Sciences, Chicago 60607, United States of America; berkelha@uic.edu

[8] Physical Research Laboratory, Faculty of Geoscience, Gujarat 380009, India; shraddha.band@gmail.com; myadava@prl.res.in

[9] Physical Research Laboratory, Faculty of Geoscience, Gujarat 380009, India; `Deceased'

* Correspondence: nkaushal@ntu.edu.sg; Tel.: +65 6908 3366

Abstract: As one of the most prominent seasonally recurring atmospheric circulation patterns, the Asian Summer Monsoon (ASM) plays a vital role for the life and livelihood of about a third of the global population. Changes in the strength and seasonality of the ASM significantly affect the region, yet the drivers of change and the varied regional responses of the ASM are not well understood. In the last two decades, there have been a number of studies reconstructing the ASM using stalagmite-based proxies such as oxygen isotopes ($\delta^{18}O$). Such reconstructions allow examination of the drivers and responses, increasing monsoon predictability. In this review paper, we focus on stalagmite $\delta^{18}O$ records from India at the proximal end of the ASM region. Indian stalagmite $\delta^{18}O$ records show well dated, high amplitude changes in response to the dominant drivers of the ASM on orbital to multi-centennial timescales and indicate the magnitude of monsoon variability in response to these drivers. We examine Indian stalagmite records collated in SISAL_v1 (version 1) database (http://researchdata.reading.ac.uk/139/) and support the database with a summary of record quality and regional climatic interpretations of the $\delta^{18}O$ record during different climate states. We highlight current debates and suggest the most useful time periods (climatic events) and locations for further work using tools such as data-model comparisons, spectral analysis methods, multi-proxy investigations and monitoring work.

Keywords: speleothem; oxygen isotopes; monsoon; paleoclimate; India; SISAL; ISM; ASM

Peer-reviewed version available at Quaternary 2018, 1, 29; doi:10.3390/quat1030029

1. Introduction

The Indian Summer Monsoon (ISM) is part of the Asian Summer Monsoon (ASM) and provides ca. 70% of India's annual precipitation. Monsoon variability results in frequent floods and droughts that significantly affect livelihood and agriculture. The latter depends on the regularity of the ISM's rainfall, intensity, seasonality, timing of onset and retreat [1]. Yet, this variability and changes in rainfall seasonality remain poorly understood [1,2]. Speleothems (mostly stalagmites) provide high resolution, multi-proxy records of ASM variability with increasingly tight age control (e.g., [3,4]). Although there is a large body of studies from Eastern Asia [5–8], the Indian subcontinent remains much less well studied. The incongruent spatial coverage between the two regions is mainly due to the availability of karst regions with suitable sampling material. Since 2004, a number of stalagmite-based proxy records of ISM dynamics have been published from 21 cave sites (Figure 1 and Table 1) in India. The available stalagmite records show that the amplitude of monsoon variability, even within the last millennium, is higher than that captured by short instrumental records [9,10] and provides evidence of multi-year to multi-decadal droughts that line up reasonably well with historical and archaeological records of droughts, famines and social disruptions [10–12]. Records further show that dynamics internal to the Earth's climate system can cause changes of the same order of amplitude as orbital forcing [13]. While dynamic climate models do not generally capture internal monsoon dynamics, spectral analysis of reconstructed monsoon time series' provide evidence of recurring low frequency monsoonal variability with timescales that are inconsistent with known external forcing mechanisms. Phase studies indicate that the ISM is sensitive to global forcings and atmospheric dynamics, including insolation [13], El Niño Southern Oscillation (ENSO) and Pacific Decadal Oscillation (PDO) dynamics [14], and changes triggered in the North Atlantic realm [13,15–17]. While individual stalagmite records have significantly increased our understanding of past monsoon variability, the drivers and pathways of ISM variability, regional responses to changes in the monsoon and the interpretation of the $\delta^{18}O$ proxy are still debated [2].

Stalagmite $\delta^{18}O$ records from the ISM region reflect the sum of several processes at any given site, including changes in larger circulation patterns, rainfall seasonality, amount and temperature, and not merely changes in local precipitation amount [18,19]. Consequently, stalagmite $\delta^{18}O$ provides a powerful proxy for the reconstruction of past circulation changes in response to orbital and North Atlantic forcings, but its meaning at local scale must be established with great care. Reconstruction of past sub-continental climate variability has been hampered by insufficient understanding of proxy-influencing factors, record quality (given rapid advances in stalagmite research), lack of spatial and temporal coverage, and synthesis of records that would enable pan-regional comparisons. This collation and synthesis of stalagmite $\delta^{18}O$ records has been made available by the SISAL (Speleothem Isotope Synthesis and Analysis) database.

The SISAL database has been created by the SISAL Working Group supported by PAGES (Past Global Changes) (http://pastglobalchanges.org/ini/wg/sisal). SISAL aims to compile and synthesize stalagmite $\delta^{18}O$ and $\delta^{13}C$ records to develop a global database which can be used to explore past climate changes and to enable climate model evaluation. The first version of the database, SISAL_v1, is available at http://researchdata.reading.ac.uk/139/. Database structure and access have been detailed in Atsawawaranunt et al [20]. The following review article is one of a series of regional review articles that support the SISAL database. $\delta^{18}O$ and $\delta^{13}C$ data of stalagmites along with relevant age and cave information are available in the database. However, less is understood of the control on $\delta^{13}C$ in stalagmites from India and it is rarely interpreted [17]. Similarly, stalagmite trace element ratios are emerging as a powerful set of proxies from stalagmites, however, trace element ratios have not been incorporated in SISAL_v1 and are only recently being explored in India. For these reasons, the following review paper focuses entirely on $\delta^{18}O$ records.

The following review supplements the SISAL database by introducing the geography and modern climate of the ISM region (Section 2), describing the spatial and temporal distribution and quality of stalagmite $\delta^{18}O$ records in the ISM region (Section 3), providing regional interpretations of the $\delta^{18}O$ records (Section 4) and discussing specific climate events and underlying forcings in the ISM region (Section 5).

Peer-reviewed version available at Quaternary 2018, 1, 29; doi:10.3390/quat1030029

2. Study Region

The most distinctive physical features of India are the Himalayan mountain range to the north and the Indian Ocean to the south of peninsular India, with the Arabian Sea in the west, and the Bay of Bengal to the east (Figure 1). Both coasts of peninsular India are characterized by mountain ranges. The ~2500 m high Western Ghats that run along the Arabian Sea coast form an orographic boundary for moisture carried from the Arabian Sea while the Eastern Ghats are lower (~1500 m) and less continuous. The Vindhyan and Satpura mountain ranges and the Chota Nagpur Plateau to the North have elevations of 700 to 1500 m and form a loose northern boundary to peninsular India.

Four climatological seasons have been designated for the ISM region (The Indian Meteorological Department):

1. Winter lasting from December until March; snowfall is seen only in the high-altitude Himalayan region. Winter climate is characterized by dry conditions through most of the other regions, with influence of north-easterly cold air masses originating on the Tibetan Plateau, the 'Winter monsoon'. In northwest India, recycled moisture from the Atlantic, Mediterranean, and near East can be introduced by the Westerlies ('Western disturbances') [21].
2. Summer or Pre-monsoon season lasting from April to June; these are the hottest and driest months of the year with temperatures increasing to the ranges of 20-40^{0}C.
3. Summer Monsoon (Indian Summer Monsoon – ISM) or rainy season lasts from July to September; the monsoon rainfall onset is as early as the first week of June in south peninsular India gradually extending across the rest of India by the first week of July. The summer monsoon season is dominated by the southwest monsoon that delivers ~70% of the total annual rainfall to India. The Meghalaya Plateau in northeast India receives exceptional amounts of precipitation at this time due to its position as the first orographic barrier for moist air masses from the Bay of Bengal [22], leading to its denomination as the 'wettest place on Earth' [23].
4. The Post-monsoon lasts for the two months of October and November; little rain is observed at this time in peninsular India with the exception of the southeast corner of India which receives most of its rain from northeast winds that source moisture from the Bay of Bengal.

The seasonal reversal of meridional temperature and pressure gradients and associated circulation pattern which constitute the summer and winter monsoons is the most outstanding feature of the Indian meteorology [24]. During the ISM period, convective rainfall dominates India's weather. A high temperature gradient between Central Asia and the Indian Ocean accompanied by the northward shift of the Inter-Tropical Convergence Zone (ITCZ) result in the Southeast trade winds turning westerly due to Coriolis forces as they cross the equator. These winds carry copious amounts of water from the Indian Ocean to peninsular India. This southwest monsoon can be depicted as two branches, the Arabian Sea branch and the Bay of Bengal branch (Figure 1). The Arabian Sea branch blows eastward across peninsular India and towards the Himalayas and has a much stronger impact on peninsular India. The Bay of Bengal branch initially tracks the eastern coast and then swerves northwest at the Himalayan orographic barrier and proceeds over the Indo-Gangetic plain. Part of the Bay of Bengal branch is pushed northwards along the deep meridionally oriented river valleys and onto the southern Tibetan Plateau. During winter, the southward retreat of the ITCZ and parallel development of the Tibetan winter high pressure cell result in a reversal of the wind patterns.

Two external factors known to affect inter-annual ISM variability over the modern instrumental period include the El Niño Southern Oscillation (ENSO) and the Himalayan/Eurasian snow cover [1]. Negative anomalies in ENSO are strongly correlated with reduced monsoon rainfall [25–27]. Historical records show that droughts associated with reductions in the amount of ISM rainfall are more closely linked to Sea Surface Temperatures (SSTs) in the central rather than the eastern equatorial Pacific Ocean [28,29]. Satellite snow cover estimates indicate a negative relationship between snow cover (snow mass) and the ISM. Excessive snow during preceding winter is unfavorable for the subsequent monsoon season because of delayed build-up of low pressure cells over the continent in spring [30–34]. However, in recent decades observations have shown that the

Peer-reviewed version available at Quaternary 2018, 1, 29; doi:10.3390/quat1030029

ENSO-ISM relationship [26,27,35] and the snow cover-ISM relationship [33] may have been weakening. The factors causing this weakening and the current dominant drivers of inter-annual variability are still debated.

A substantial component of ISM variability on annual scale stems from intra-seasonal oscillations in monsoon precipitation termed active-break periods which exhibit a hierarchy of quasi periods (8-7 days, 10-20 days, 30-60 days) [1,36]. During an 'active' period a positive rainfall anomaly is found over western and central India and a negative rainfall anomaly over northeast and southeast India. During a 'break' period, the signs are reversed [37,38]. Although questions remain regarding the mechanisms that drive inter-annual variability in the frequency of active-break cycles, their individual manifestations appear to be associated with the Madden-Julian Oscillation (MJO), which is the dominant driver of sub-seasonal climate variability in the pan-tropics [39]. Less is known of the controls on decadal variability in the ISM. Studies suggest that solar irradiance [40] and Pacific Ocean SST's [40,41] influence ISM multi-decadal variability.

3. Distribution of Speleothem Isotopic Records in Space and Time

The spatial distribution of currently known stalagmite $\delta^{18}O$ records in SISAL_v1 as well as from publications and conference abstracts (published by April, 2018) from the ISM region is shown in Figure 1. Table 1 provides a comprehensive list of published records and indicates whether the records are available in SISAL_v1. Mirroring the distribution of karst in India, most stalagmite records are from the northern and northeastern Himalayas. Few records have been recovered from central and southern peninsular India and there are no known records from the northwest and the Indo-Gangetic plains. The oldest and longest published stalagmite record is from Bittoo cave in northern India covering the last 240 ka [13]. Orbital, millennial and Holocene scale records are available from the ISM region but most of the records are discontinuous and cover relatively brief snapshots of time (Figure 2). Nevertheless, $\delta^{18}O$ covering time periods of climatic significance are available from north, northeast and peninsular India (Figure 3). Further information on the spatio-temporal distribution of stalagmites and details on the potential for further work from these caves is given in sections 3.1 and 3.2, while section 3.3 provides information on the quality of the records.

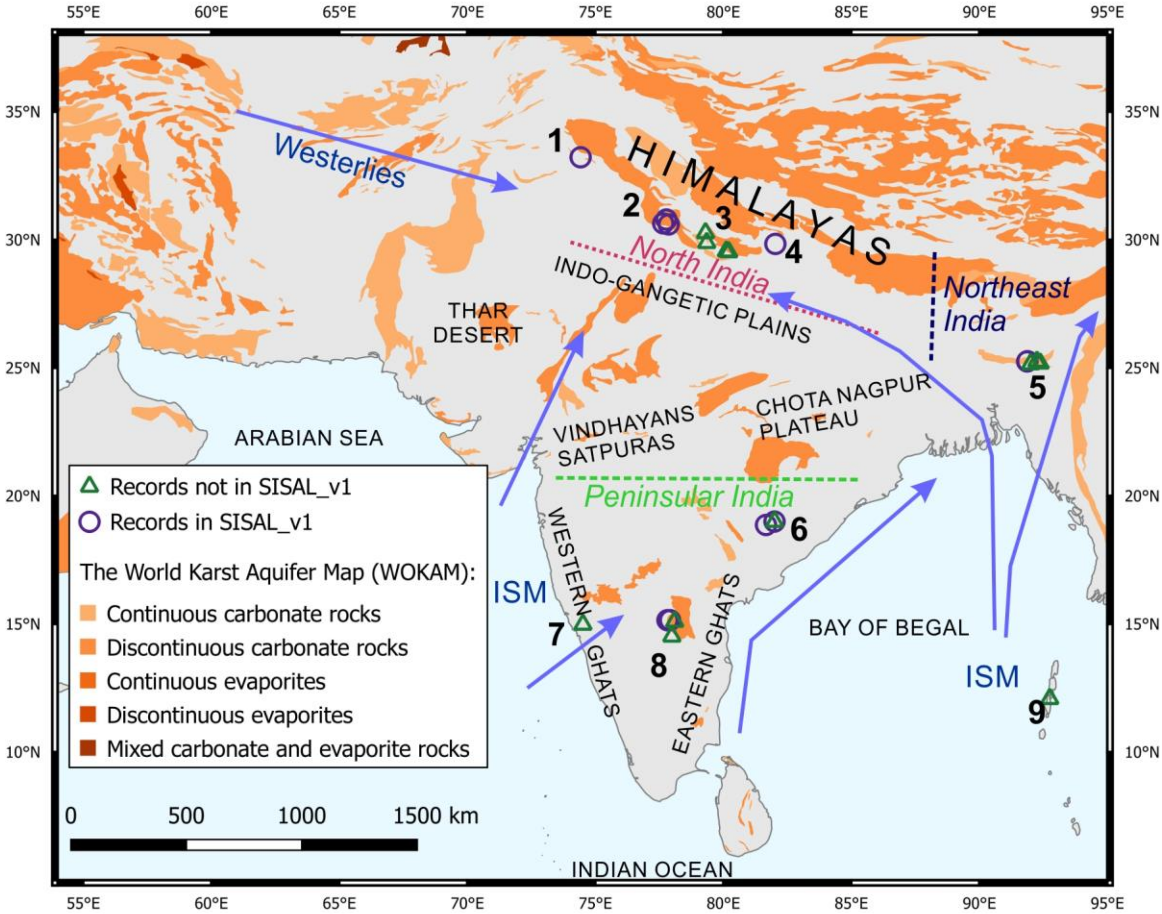

Figure 1. Study area with carbonate rock distribution as given by The World Karst Aquifer Map (WOKAM [42]) (see map legend), generalized wind directions (ISM and Westerlies marked by blue arrows), geographical features, regions (north, north-eastern and peninsular Indian) and cave locations (1: Kalakot. 2: Bittoo, Sahiya, Tityana. 3: Chulerasim, Dharamjali, Panigarh, Sainji. 4: Timta. 5: Mawmluh, Rupasor, Syndai, Umsynrang, Wah Shikhar. 6: Dandak, Jhumar, Kotumsar. 7: Akalagavi. 8: Belum, Munagamanu, Nakarallu, Valmiki. 9: Baratang.)

Preprints (www.preprints.org) | NOT PEER-REVIEWED | Posted: 19 September 2018 doi:10.20944/preprints201809.0380.v1

Peer-reviewed version available at *Quaternary* **2018**, *1*, 29; doi:10.3390/quat1030029

Table 1. List of stalagmite δ18O records from the ISM region.

site_name	*site_id*	*latitude* N	*longitude* E	*elevation* m amsl	*entity_name*	*entity_id*	Min. Year BP	Max. Year BP	Reference
Bittoo cave	1	30.79	77.78	3000	BT-1	1	12209	56236	Kathayat et al., 2016 [13]
					BT-2.1	2	24957	43676	Kathayat et al., 2016 [13]
					BT-2.2	3	43675	58310	Kathayat et al., 2016 [13]
					BT-2.3	4	58310	179204	Kathayat et al., 2016 [13]
					BT-2.4	5	179280	191449	Kathayat et al., 2016 [13]
					BT-2.5	6	227021	234000	Kathayat et al., 2016 [13]
					BT-4	7	271150	283817	Kathayat et al., 2016 [13]
					BT-6	8	199872	225988	Kathayat et al., 2016 [13]
					BT-8	9	874	3477	Kathayat et al., 2016 [13]
					BT-9	10	243063	265735	Kathayat et al., 2016 [13]
Dandak cave	130	19.00	82.00	400	DAN-D	278	387.9	1325.25	Berkelhammer et al., 2010 [43] Sinha et al., 2007 [9]
Jhumar cave	153	18.87	81.67	600	JHU-1	328	-58	873.78	Sinha et al., 2011 [11]
Kalakot cave	43	33.22	74.43	826	KL 3	119	9645	16322	Kotlia et al., 2016 [44]
Mawmluh cave	12	25.26	91.88	1160	KM-A	61	3653	12395	Berkelhammer et al., 2013 [45]
					MWS-1	62	5532	33788	Dutt et al., 2015 [16]
					MAW-6	63	6510	15907	Lechleitner et al., 2017 [17]
							-62	-16.4	Myers et al., 2015 [14]
							6600	22700	Huguet et al., 2018 [46]

Munagamanu cave	157	15.15	77.92	475	Mun-stm2	348	-59.06	3852.2	Genty et al., unpublished [47]
					Mun-stm1	349	-54.71	694.88	Genty et al., unpublished [47]
Sahiya cave	54	30.60	77.87	1190	SAH-AB	132	-59.06	3852.2	Sinha et al., 2015 [10]
							2080	5684	Kathayat et al., 2017 [12]
Timta cave	61	29.84	82.03	1900	T1	145	11664	15215	Sinha et al., 2005 [15]
Tityana cave	126	30.64	77.65	1470	TC1	262	1580	3907	Joshi et al., 2017 [48]
Valmiki cave	28	15.15	77.82	420	VSPM 1	99	13161	15607	Raza et al., 2017 [49]
					VSPM 4	100	14697	15696	Lone et al., 2014 [50]
Wah Shikhar cave	64	25.25	91.87	1290	WS-B	148	-56.65	551	Sinha et al., 2011 [11]
Akalagavi cave		14.98	74.52	521			-47	284	Yadava et al., 2004 [51]
Baratang cave		12.08	92.75	20			~0	~3300	Laskar et al., 2011 [52]
							~0	~800	Laskar et al., 2013 [53]
							~800	~3700	Laskar et al., 2013 [53]
Belum cave		15.1	78.1	367			~99000	~108000	Allu et al., 2014 [54]
Chulerasim cave		29.89	79.35	1254			0	328	Kotlia et al., 2016 [55]
Dharamjali cave		29.52	80.21	2200			-60	1780	Sanwal et al., 2013 [56]
Kotumsar cave		19.00	82.00	32			~5600	~8400	Band et al., 2018 [57]
							1964	3218	Kaushal et al., unpublished (Supplementary Materials)

Peer-reviewed version available at Quaternary 2018, 1, 29; doi:10.3390/quat1030029

Nakarallu cave		14.52	77.99	280			~1700	~3300	Sinha et al., 2017 (EGU Abstract) [58]
Panigarh cave		29.55	80.12	1520			-55	694	Liang et al., 2015 [59]
Sainji cave		30.27	79.30	1478			200	~4000	Kotlia et al., 2014 [60]
Umsynrang cave		25.18	92.37	875			~0	~11000	Breitenbach, 2009, PhD thesis [61]

3.1. Spatial distribution of caves and potential for paleoclimate studies

A comprehensive data collation of north and northeast Indian caves is provided by Gebauer [62–70] and Breitenbach and Gebauer [71] published in the Berliner Höhlenkundliche Berichte (www.speleo-berlin.de). A number of publications provide further information on the karst and caves of the north and northeast region [72–77] .

In comparison to the Himalayan region, very limited information is available on the caves from peninsular India. Karst caves in peninsular India are mainly found in the Proterozoic Mahanadi, the Kaladgi and the Cuddapah basins. Dandak, Jhumar, Gupteshwar, Kailash and Kotumsar caves are a part of the Mahanadi basin. Additional information on caves from the Mahanadi basin can be found in [78–80]. This region is worth exploring further but the current disturbed political conditions prevent exploration. Akalagavi cave has formed in the limestone and dolomite formations of the Kaladgi basin on the west coast of India. Several other caves from the same karst region have been explored. Akalagavi and one other cave are currently dripping but no stalagmites suitable for further paleoclimate work are observed from this region. Belum, Valmiki, Munagamanu and Nakarallu are located in the Cuddapah basin. Dar et al. [81], have published a comprehensive review of the Cuddapah karst region from peninsular India. This region is worth exploring further for paleoclimate records. Several caves are protected for tourism and as temple caves. Bora cave is a part of the Eastern Ghats Mobile Belt of Precambrian age. Although well decorated, it is a large, open, airy cave and is unlikely to be suitable for paleoclimate work. No other caves are reported from this region. Baratang cave is located in limestone formations of Cenozoic age in the Andaman Island in the Bay of Bengal.

3.2. Temporal distribution of stalagmite paleoclimate records

Figure 2 shows the temporal distribution of stalagmite $\delta^{18}O$ records from India in SISAL_v1. Table 1 provides information on records published from this region, including those records not currently in the SISAL database. Orbital scale records are available from Bittoo cave [13] from north India and Belum cave [54] from peninsular India. Mawmluh cave [16,17,46] from the northeast currently covers the Last Glacial Maximum, and Heinrich stadials. Records from peninsular Valmiki cave covers the later phase of Heinrich event 1 [50] and the last deglaciation [49]. Bittoo [13], Kalakot [44] and Timta [15] caves from north India and Mawmluh [16,17,46] cave from northeast India cover the Bølling-Allerød (BA) and Younger Dryas (YD) periods. Sahiya [10,12] cave from north India, Mawmluh [45] and Umsynrang [61] caves from northeast India and Kotumsar [57] cave from peninsular India encompass significant periods of the Holocene. The other published records listed in Table 1 cover brief snapshots of time of the last 5000 years.

Peer-reviewed version available at Quaternary 2018, 1, 29; doi:10.3390/quat1030029

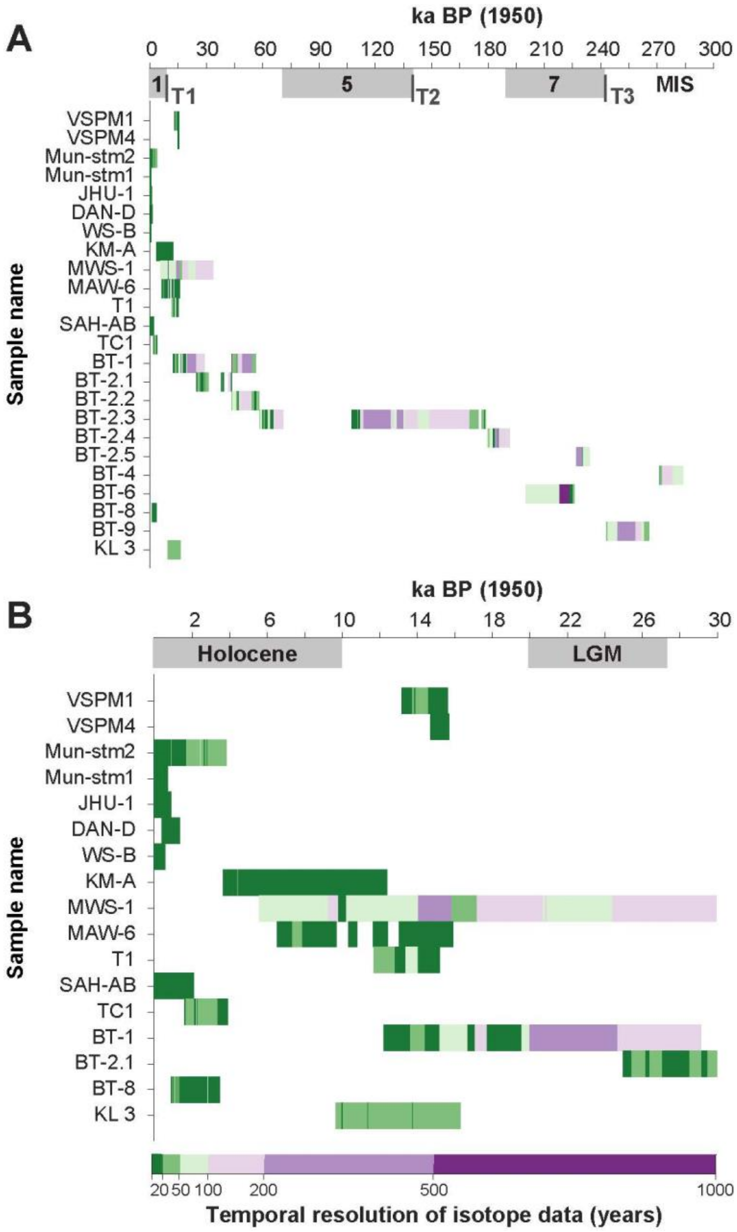

Figure 2. Temporal distribution of stalagmite δ¹⁸O records from India in SISAL_v1. Age in ka BP has been given on the x-axis. The two figures cover ages (a) 300 to 0 ka BP and (b) 30 to 0 ka BP respectively. The color bar indicates the temporal resolution of isotopic data (years). The y-axis gives the record's ID (entity_name) as found in the database. VSPM1 and VSPM4 from Valmiki cave. Mum-stm2 and Munstm-1 from Munagamanu cave. JHU-1 from Jhumar cave. DAN-D from Dandak cave. WS-B from Wah Shikhar cave. KM-A, MWS-1 and MAW-6 from Mawmluh cave. T1 from Timta cave. SAH-AB from Sahiya cave. TC1 from Tityana cave. BT-1 to BT-9 from Bittoo cave. KL3 from Kalakot cave. Further details can be found in Table 1.

Preprints (www.preprints.org) | NOT PEER-REVIEWED | Posted: 19 September 2018 doi:10.20944/preprints201809.0380.v1

Peer-reviewed version available at Quaternary 2018, 1, 29; doi:10.3390/quat1030029

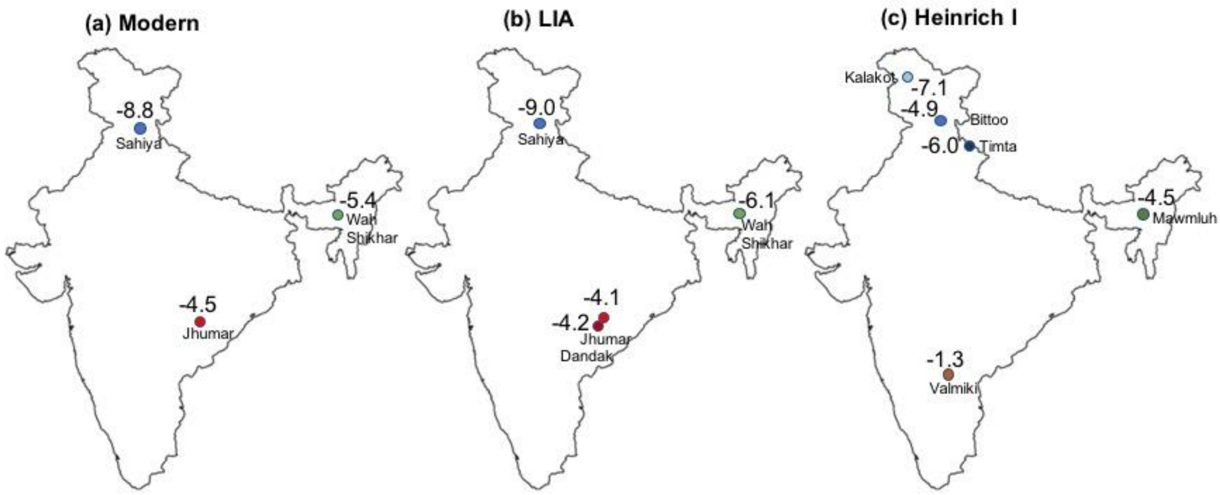

Figure 3. Spatial distribution of stalagmite δ[18]O records from India in SISAL_v1 during three time slices (a) Modern from 0 to -55 years BP, (b) Little Ice Age (LIA) from 551 to 387 years BP and (c) Heinrich I from 15215 to 14697 years BP. The choice of age ranges for the various time slices reflect availability of records (see Figure 2). The standard deviation on all records was 0.5‰ or less apart from the Bittoo cave record for Heinrich I with a standard deviation of 1.3‰. The Valmiki cave stalagmites are composed of aragonite and may require a +0.8‰ correction to be compared with the other records from calcite stalagmites (see section 3.3).

3.3. Quality of the records

The interpretation of a δ[18]O time series strongly depends on the temporal resolution and chronological precision of the stalagmite record. Keeping this in mind, the quality of the records can be assessed based on a few objective parameters such as speleothem form, mineralogy, age control, sampling density (resolution) and cave monitoring, which aids in the interpretation of the δ[18]O signal. The SISAL database provides information on all these parameters and aids in the selection of appropriate stalagmite δ[18]O records to reconstruct ISM variability on different timescales. One further parameter i.e. age uncertainty envelopes on records, need to be carefully discussed since statistical comparability between records is hampered by the lack of uncertainty information in publications and the lack of knowledge of the difference in uncertainty envelopes when using different age models. Only a few points from stalagmite samples are dated within a proxy record and various age models are then employed for giving an age-depth relationship for each proxy data point. Age modeling techniques (e.g. [82–85]) propose methods to calculate uncertainties between dated points allowing for continuous error propagation and the true uncertainty envelope of a time series to be established. The SISAL database will address this issue by calculating and discussing the uncertainty envelopes for the large number of records available in the database (work in progress) providing a precise way to statistically compare records. Pending the publication of the SISAL age model paper, this review paper on Indian stalagmites simply considers individual age errors (uranium-thorium or radiocarbon ages) for the records.

The longest Indian record (ca. 240 ka) is from Bittoo cave, a composite record of ten stalagmites from the same cave [13]. Replication of δ[18]O patterns by multiple stalagmites greatly increases the confidence in the climatic signal of the proxy signal. However, the record shows multiple hiatus periods that limit the availability of δ[18]O values for certain climate states.

Global-scale climate events such as the Heinrich, the BA, the YD, the 4.2 ka event and the Little Ice Age (LIA) events have typically lasted for 50-1000 years. When detectable, the amplitude of δ[18]O excursions of these events is low (~1 to 2‰) compared to glacial-interglacial variability in the available records. Examination of such events requires tight age control and high confidence in the climatic influence on the δ[18]O record. The Bittoo [13], Kalakot [44], Timta [15] and Mawmluh [16,17] cave records provide measurements of δ[18]O covering the BA and YD periods. The Bittoo and Timta

Preprints (www.preprints.org) | NOT PEER-REVIEWED | Posted: 19 September 2018 doi:10.20944/preprints201809.0380.v1

Peer-reviewed version available at Quaternary 2018, 1, 29; doi:10.3390/quat1030029

cave stalagmites from north India provide better age control (Figure 5) than the Kalakot record. The Bittoo and Mawmluh cave records also provide $\delta^{18}O$ measurements of multiple Heinrich stadials. The Valmiki cave record [50] from peninsular India covers the later part of Heinrich I but does not replicate with a second Valmiki cave record [49] and needs to be treated with caution (Figure 4 in supplementary material). The Valmiki stalagmites are composed of aragonite rather than calcite. Under equilibrium conditions, aragonite should have $\delta^{18}O$ values 0.8‰ higher than calcite at 25^{0}C [86]. This 0.8‰ offset in $\delta^{18}O$ records between calcite and aragonite stalagmites has to be reckoned with when considering or comparing $\delta^{18}O$ records over large spatial scales for modeling studies. Stalagmites composed entirely of aragonite have several benefits, such as a tendency to contain high uranium concentrations and high growth rates which provide high resolution records with tight age control (see [87]), and are being increasingly studied. However, at present, less is known about conditions governing $\delta^{18}O$ in aragonitic stalagmites compared to calcitic stalagmites.

The Mawmluh cave record covering the 4.2 ka event [45] provides sufficient age control with low errors of ±40-60 years. The Mawmluh cave $\delta^{18}O$ records are supported by robust monitoring studies [22,88] that significantly increases confidence in the interpretation of the stalagmite $\delta^{18}O$ records from this cave. However, there is lack of replication in the Mawmluh cave records [16,17,45] over short time periods and therefore these records must be treated with caution when examining millennial and shorter time scale events (Figure 5).

Figure 2b indicates that Sahiya [10], Wah Shikhar [11], Dandak [9], Jhumar [11] and Munagamanu [47] cave records provide $\delta^{18}O$ data of the entire or part of the LIA event beginning around 750 to 450 years BP (1200 to 1500 CE) [89,90]. The Sahiya cave record has been constructed with tight age control (errors of ±40 years over the LIA period) and replicate $\delta^{18}O$ records for significant time periods [10,12] making it a reliable climate record to examine the LIA for north India. The high resolution Dandak and Jhumar cave records from peninsular India similarly provide the most reliable record of the LIA for this region [9,11,43]. Although the chronology of the Jhumar cave record is not independently well constrained, its replication with the Dandak cave record from the same region provides confidence in its interpretation. With age errors of ±200 years the Wah Shikhar cave record from the northeast provides limited age control for examining the LIA. The chronology of the Munagamanu cave record is fairly robust but shows mixed calcite and aragonite mineralogy which hampers interpretation of the LIA $\delta^{18}O$ record. Care needs to be taken with mixed calcite-aragonite samples because the cause of variation in the $\delta^{18}O$ record maybe due to climatic/environmental factors, or changes in mineralogy, or a combination of both.

There are a few records that are not available in SISAL_v1 that have been referred to in this paper (Table 1). Of these, the Panigarh [59] and Sainji [60] stalagmites show mixed calcite-aragonite mineralogy while Mawmluh [14], Akalagavi [51], Chulerasim [55], Umsynrang [61], and Dharamjali [56] stalagmites are composed of aragonite. A few records provide useful $\delta^{18}O$ measurements for certain time intervals but lack age control to examine events closely, such as the Tityana [48], Akalagavi [51], Belum [54] and Baratang [52,52] cave records.

4. Regional Patterns in Speleothem Oxygen Isotope Records and their Climatic Interpretations

In this section, examples for proxy calibration using instrumental climate data from all three ISM regions, i.e. north, northeast and peninsular India, have been introduced. However, past climate states are likely to have varied and circulation patterns were different from today's. Keeping this in mind, in the following we address the current level of understanding and existing debates.

4.1. North India

Paired analysis of GNIP (Global Network of Isotopes in Precipitation) $\delta^{18}O_{rainfall}$ data collected at Delhi and low level wind trajectory patterns show that $\delta^{18}O$ variability in northern India is linked to periods of strong (weak) ISM circulation [10]. Strong (weak) ISM periods are characterised by enhanced (reduced) flux of isotopically depleted Bay of Bengal moisture and reduced (enhanced) flux of isotopically enriched Arabian Sea moisture [10]. As stalagmites are ultimately fed by rainwater,

$\delta^{18}O_{stalagmite}$ reflects such changes in ISM circulation dynamics. This interpretation hinges on strong seasonality and the premise that effective precipitation is positive only during the ISM but negative during the rest of the year [10]. However, seasonality changes in the past might have altered this climate state, thus complicating the interpretation of $\delta^{18}O_{stalagmite}$. For example, a negative $\delta^{18}O$ excursion found in multiple stalagmites from north India is interpreted to be a result of stronger winter Westerly Disturbances and weaker ISM circulation during the entire or part of the LIA (e.g. [55,56,60]). However, the influence of Westerly disturbances on stalagmite $\delta^{18}O$ records is debated (see Section 5). In most scenarios, it is thought that winter season infiltration is minimal and does not contribute significantly to the $\delta^{18}O$ budget of infiltrating waters [10,88].

Phase correspondence of stalagmite $\delta^{18}O$ records from this region with millennial events thought to have been triggered in the North Atlantic [12,15] and the bi-polar see-saw pattern observed with Antarctic ice core records [13] constitute strong evidence for an impact of hemispheric-scale circulation on stalagmite $\delta^{18}O$ records. Rapid positive excursions in the Bittoo stalagmite $\delta^{18}O$ record corresponding with events identified in the Greenland (NGRIP) ice core record ~55 ka, at a time when Antarctic ice cores show low amplitude warming suggests a dominant Northern Hemisphere forcing at millennial scale in this region [13]. Phase correspondence with Northern Hemisphere Summer Insolation (NHSI), with abrupt and high amplitude (~4‰) negative $\delta^{18}O$ excursions in the Bitoo cave stalagmite, suggests direct insolation forcing of the ISM [13]. Further, the well-dated MIS-5 and MIS-3 portions of the Bittoo cave record show no visible phase difference with its counterparts in the East Asian Monsoon (EAM) domain [8,91] indicating that speleothem $\delta^{18}O$ variations are broadly in phase in the peripheral ISM and EAM domains.

4.2. Northeast India

Back trajectory analysis shows that the Bay of Bengal is the dominant source of moisture for northeast India [22]. Two years of observation reveal a trend toward lighter $\delta^{18}O$ in the late ISM in connection with temporal variations in river runoff into the Bay of Bengal that might contribute up to 25% of observed changes in $\delta^{18}O$ of precipitation in this region [22]. Rainfall data collected by Breitenbach et al. [22] has been used to validate a synthetic multi-decadal $\delta^{18}O$ time-series generated from an isotope-enabled General Circulation Model (GCM) (after [92]) by Berkelhammer et al.[45]. The synthetic time-series suggests that there is significant negative correlation between $\delta^{18}O$ and rainfall amount only when the late ISM rainfall (October in addition to JAS) is included, suggesting that the amount effect is a result of a prolonged ISM rainfall season [45]. The studies suggest that more positive stalagmite $\delta^{18}O$ values from the region may indicate early monsoon onset or early withdrawal or both in addition to changes in and at moisture source and transport pathways.

Instrumental data shows that in contrast to central peninsular India, rainfall amounts in northeast India are relatively unaffected by ENSO dynamics [22]. Despite this, El Niño years are marked by more positive $\delta^{18}O$ values in a sub-annually resolved, 50-year long aragonite stalagmite $\delta^{18}O$ record from Mawmluh cave [14]. Back trajectory analysis by Myers et al.[14], indicates that during Central Pacific- El Niño events, moisture transport distance to northeast India is reduced giving more positive rainwater $\delta^{18}O$ values and can be detected by the weak but significant positive correlation between this stalagmite $\delta^{18}O$ and central Pacific SST's. In addition, the $\delta^{18}O$ record shows significant correlation with Pacific decadal variability.

Glycerol Dialkyl Glycerol Tetraether (GDGT) [46], $\delta^{13}C$ and ice volume corrected $\delta^{18}O$ [17] measured from stalagmites in this region give additional information on the controls on $\delta^{18}O$ variation. For example, the ice volume corrected $\delta^{18}O$ suggest that ice volume and SST changes account for only 1/4th (~1‰) of the $\delta^{18}O$ change from the glacial to deglacial, the larger part is attributable to change in ISM strength [17]. Similarly, the temperature reconstruction given by the stalagmite GDGT proxy indicates little temperature change in this region during the YD event. This suggests that $\delta^{18}O$ variation is not controlled by local temperature change but by larger circulation changes triggered by a distal North Atlantic event [46]. And the coupled analysis of $\delta^{18}O$ and $\delta^{13}C$ further indicate that the $\delta^{18}O$ variation between the BA and into the YD may be more representative of a change in seasonality of rainfall associated with a weaker ISM [17].

On orbital time scales, the Umsynrang Holocene $\delta^{18}O$ record shows an inverse relationship with insolation. The period of maximum rainfall and enhanced seasonality corresponds to the Holocene Thermal Maxima observed in Europe [61].

4.3. Peninsular India

Monsoon trajectory analysis [57] suggests that the Arabian Sea (and probably continental recycling) is the dominant source of moisture for the monsoon rainfall period (JJAS) while the Bay of Bengal, the Indian Ocean and continental recycling are minor sources of moisture that play a role only during the remaining months. The Jhumar cave $\delta^{18}O$ record overlaps with the instrumental period and shows a significant inverse relationship with a regional (18^0 - 27^0N and 69^0 – 88^0E) JJAS precipitation time series (1903-2005 AD, n = 70, R^2 = -0.21) suggesting that $\delta^{18}O$ variations from this location reflect rainfall amount [11]. Similarly, there is significant negative correlation of R^2 = (-)0.38 between decadally averaged Akalagavi stalagmite $\delta^{18}O$ (measured at annual resolution) and the regionally averaged instrumental rainfall amount data (n=89) [51]. These two studies suggest that at least some part of the variance in stalagmite $\delta^{18}O$ results from changes in the amount of regional and upstream rainfall, but other drivers of $\delta^{18}O$ variation need to be considered as well. This interpretation has been used to explain past variation in stalagmite $\delta^{18}O$ from this region on millennial and orbital time scales as well but requires verification through data-model comparisons. For example, stalagmite $\delta^{18}O$ records from this region suggest that the Medieval Warm Period (MWP) was a wet period while the early LIA was characterised by multi-decadal droughts [9,11]. A coupled study with Wah Shikhar cave located in northeast India proposes that the period from 550 to 250 years BP was marked by higher frequency and/or amplitude break events which cumulatively generate a negative precipitation anomaly over Central India [11]. It was subsequently found that the $\delta^{18}O$ record from northeast India is controlled by multiple factors other than the amount effect [22,45]. The Kotumsar $\delta^{18}O$ record similarly shows that there was a gradual decrease in the amount of rainfall from 8500 to 7300 y BP followed by an increasing trend from 7300 to 5600 y BP [57]. An aragonite stalagmite record from Valimiki cave indicates more wet climate during Termination 1a [50] and during the later phase of Heinrich event 1 [50] pending replicate measurements and verification.

5. Discussion

The available stalagmite $\delta^{18}O$ data in SISAL show that regional ISM responses differ in terms of sensitivity and timing. Better understanding of regional dynamics causing stalagmite $\delta^{18}O$ variation allows examination of specific aspects of the monsoon such as rainfall amount, source and path changes and changes in length of the season. Such regional paleoclimate records provide valuable information to test the ability of climate models to predict changes in the ISM in response to different forcing mechanisms and climate states. Based on the availability of stalagmite records from India, the following discussion sections examine regional ISM variability in response to volcanic/solar forcing during the LIA, North Atlantic and orbital-insolation drivers.

5.1. The LIA

Temperature reconstructions across the globe generally indicate a cooling trend beginning around 750-450 BP (1200-1500 CE) (inter-spread with periods of warmth) continuing into the nineteenth century and is referred to as the Little Ice Age [89,90]. A number of different forcing mechanisms such as solar and/or volcanic coupled with ocean-atmosphere feedbacks have been used to explain the LIA cooling trend (e.g. [93,94]). Paleoclimate studies have used stalagmite $\delta^{18}O$ records to understand ISM variation during the LIA. Rehfeld et al. [95], use the Akalagavi [51] and Dandak [9] records to examine the relationship between ISM and EAM using complex networks. Chen et al. [96], use the Dandak [9] and Dharamjali [56] records along with a number of other proxy records across the ASM region to suggest a 'wet-North and dry-South' pattern during the LIA. A similar conclusion is reached by Dixit and Tandon [97], who use several proxy records from the ISM region to discuss the hydroclimate of the Holocene. This section examines the LIA period using stalagmite $\delta^{18}O$ records available in SISAL_v1.

The most distinct and reliable indication of the LIA having been associated with ISM variation is given by the Dandak and Jhumar cave records from peninsular India (Figure 4). These records suggest that the LIA manifested as two successive prolonged $\delta^{18}O$ excursions covering the time period from 600 to 280 years BP (1350 to 1670 CE). The north-eastern Wah Shikhar cave record [11] conversely shows a negative $\delta^{18}O$ excursion from 520 years BP (just after the stalagmite started growing) to 250 years BP (1430 to 1700 CE). The Sahiya cave record [10] from north India shows one significant positive excursion lasting for ~25 years from 355 to 328 years BP (1595 to 1622 CE), but no evidence for a prolonged change in ISM circulation.

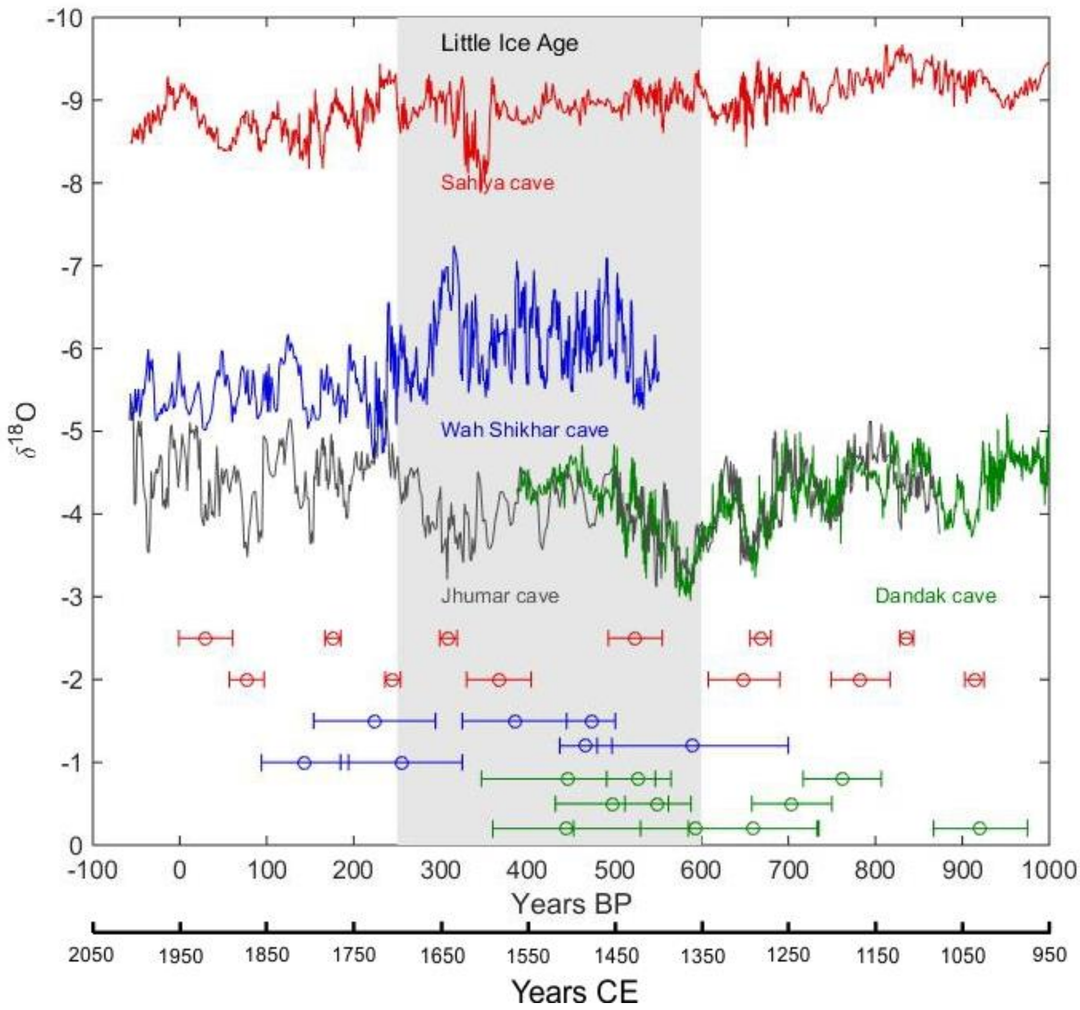

Figure 4. SISAL_v1 ISM stalagmite $\delta^{18}O$ records covering the LIA. Age in years BP has been given on the x-axis. The y-axis gives the $\delta^{18}O$ in ‰VPDB. The LIA period has been demarcated as 600 to 250 years BP (1350 to 1700 CE) (see text for details). Sahiya [10], Wah Shikhar [11], Jhumar [11] and Dandak [9] cave records have been shown along with their U-Th age errors.

These records suggest regional differences in responses to circulation changes during the LIA (Figure's 3 and 4). While ISM rainfall in peninsular India was reduced, north-eastern India experienced an increase in monsoon season length and changes in moisture source and path (see Section 4). The Sahiya record from north India suggests that LIA dynamics did not produce significant changes in ISM rainfall $\delta^{18}O$. However, three lines of evidence suggest that further work is required in the north Indian region:

1. Multiple proxy records from the north Indian region (such as lake core records) suggest change in ISM rainfall amount in north India during the LIA (e.g. [97] and references therein).

Preprints (www.preprints.org) | NOT PEER-REVIEWED | Posted: 19 September 2018 doi:10.20944/preprints201809.0380.v1

Peer-reviewed version available at Quaternary 2018, 1, 29; doi:10.3390/quat1030029

2. If changes in circulation during the LIA are a result of active-break dynamics as suggested by Dixit and Tandon [97], the northeast and north Indian cave records should respond with $\delta^{18}O$ excursions in the same direction as a result of stronger Bay of Bengal branch of precipitation.
3. If changes in circulation during the LIA are a result of a weaker ISM and stronger Western Disturbances as suggested by Kotlia et al [60] and Sanwal et al [56], then there needs to be unambiguous evidence of Western Disturbances influencing cave stalagmite $\delta^{18}O$ records (either through seasonal drip water $\delta^{18}O$ changes or cave ventilation changes) at present or in the past (e.g., through investigation in spatially separated stalagmite records and climate modelling).

5.2. North Atlantic Forcing

Arabian Sea ocean sediment records of upwelling intensity [98–100] are consistent with reduction in ISM during cold stadials, e.g., Heinrich stadials and the Younger Dryas stadial [101]. Pausata et al, use an isotope enabled Atmospheric General Circulation Model (AGCM) to show that a sudden increase in the sea ice extent in the North Atlantic region during a Heinrich stadial lead to cooling of the Northern Hemisphere, reduced precipitation over the Indian basin and weakening of the ISM. The precipitation was isotopically heavier over India at this time [102].

Nearly all stadials in the 240 ka Bittoo cave record [13] are characterised by more positive $\delta^{18}O$ values compared to interstadials, consistent with the modeling results given by Pausata et al [102]. Unlike the LIA, this pattern of more positive $\delta^{18}O$ is replicated by other shorter records from north and northeast India [15–17,44] (Figure 3). The Bittoo and Mawmluh cave records suggest that Heinrich stadials are responsible for higher amplitude changes in the ISM than the YD stadial in north and northeast India (Figure 5). However, the transition into and out of the Heinrich stadials is not as distinct as the transition into the YD. The transition to the YD occurs abruptly (within ~100 years) at 12.7 ka in the north Indian Bittoo [13], Timta [15] and Kalakot [44] records (Figure 5). Although the Kalakot cave record does not show the negative excursion of the BA seen in the other records. The Bittoo and Kalakot records mark the end of the YD within 500 years of its onset. The magnitude of change in $\delta^{18}O$ from the BA to the YD period is ~2‰ in this region. Though the northeast Indian cave records indicate the BA-YD excursions with tight age control, the $\delta^{18}O$ records from Mawmluh cave do not replicate well with each other over the BA-YD transition. One Mawmluh cave record (MWS-1) shows a sharp transition at 12.8 ka BP. The magnitude of $\delta^{18}O$ transition from BA to YD is lower than in the north Indian cave records at ~1‰.

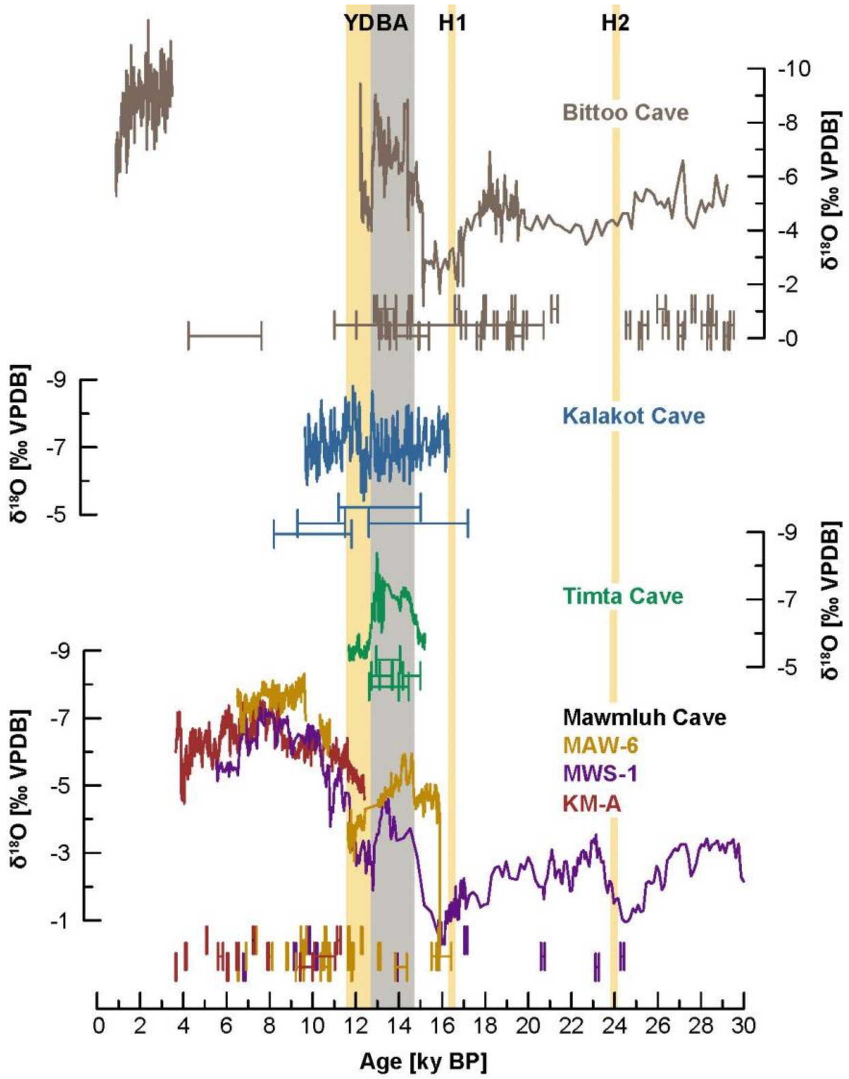

Figure 5. SISAL_v1 ISM stalagmite δ¹⁸O records covering millennial events over the last deglaciation. The Younger Dryas (YD) and Heinrich events 1 and 2 [103] are indicated by yellow bars. Bölling-Allerød (BA), is indicated by a grey bar. The BA-YD transition is marked at 12.8 ka BP in the figure (GISP2 [104]). Bittoo [13], Kalakot [44], Timta [15] and Mawmluh [16,17] records are shown along with their U-Th age errors.

5.3. Orbital Forcing

Battisti et al [19]., use an isotope enabled coupled AGCM to present a high insolation signal at 218 ka BP and a low insolation signal at 207 ka BP with a 100 W/m^2 difference between the two at 30^{0}N for June-July-August. Model results suggest that the $\delta^{18}O$ difference between the high and low insolation phases is between 4 to 6 ‰ in the north and northeast Indian region. The Bittoo cave record [13] shows a ~6‰ shift in $\delta^{18}O$ between the low insolation phase at MIS 6 and the high insolation phase at MIS 5. Similarly, the 30 ka long Mawmluh [16] cave record (Figure 6) shows a ~6‰ difference between the low insolation phase at MIS 2 and the high insolation phase at MIS 1. Further, the Mawmluh cave record of ~30 ka shows no visual phase difference with the Bittoo cave record with similar magnitude of $\delta^{18}O$ change strongly suggesting that on orbital time scales, ISM variation is in phase with solar insolation in north and northeast India. These results appear to settle previous debates on direct insolation forcing versus a phase difference between insolation forcing and ISM change [13].

Preprints (www.preprints.org) | NOT PEER-REVIEWED | Posted: 19 September 2018 doi:10.20944/preprints201809.0380.v1

Peer-reviewed version available at Quaternary 2018, 1, 29; doi:10.3390/quat1030029

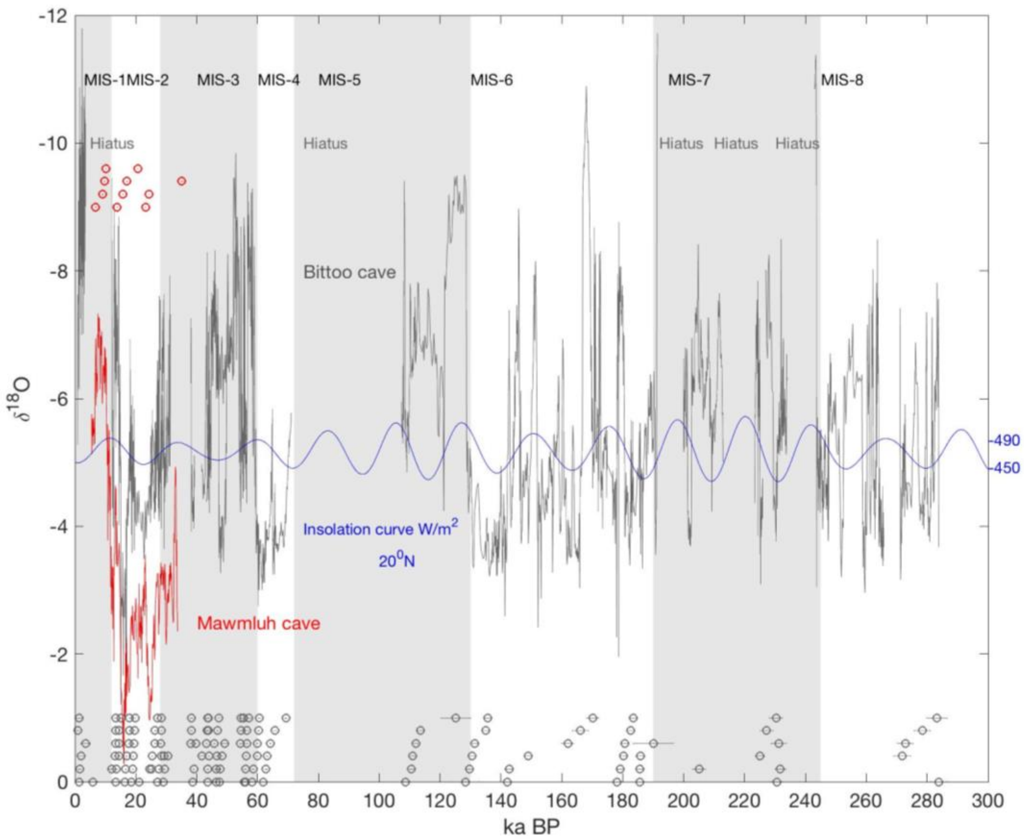

Figure 6. ISM stalagmite $\delta^{18}O$ records on orbital timescale. Bittoo [13] and Mawmluh [16] cave records are shown along with their U-Th age errors. Hiatus periods in the Bittoo cave record are marked. Marine Isotope Stages (MIS) are demarcated by grey and white bars. The insolation curve in W/m^2 at 20^0N is shown in blue [105].

The Umsynrang record [61] from northeast India is the only record that covers the entire Holocene from Indian (not in SISAL_v1). The record shows a parabolic curve peaking at ~9 ka BP with progressive increase in $\delta^{18}O$ of ~1‰ across the Holocene matching modeling studies by LeGrande and Schmidt [18] and Battisti et al. [19], which calculate a 1‰ increase in rainfall $\delta^{18}O$ associated with a 27 W/m^2 decrease in summer insolation over the Holocene. The records from Figure 7 cover parts of the Holocene. The Mawmluh cave record from northeast India similarly shows an increasing $\delta^{18}O$ trend with decreasing insolation, however it peaks later in the Holocene at ~8.5 ka BP. The Sahiya $\delta^{18}O$ cave record [12] from north India also follows the insolation curve during its 5000 years of growth. The peninsular Indian cave record is formed of two stalagmites from Kotumsar cave (KOT-[57] and NK record given in the supplementary material of this paper) and the coupled Dandak [9] and Jhumar [11] cave records but the parabolic trend seen in the other records is not as clear from this region.

Preprints (www.preprints.org) | NOT PEER-REVIEWED | Posted: 19 September 2018 doi:10.20944/preprints201809.0380.v1

Peer-reviewed version available at Quaternary 2018, 1, 29; doi:10.3390/quat1030029

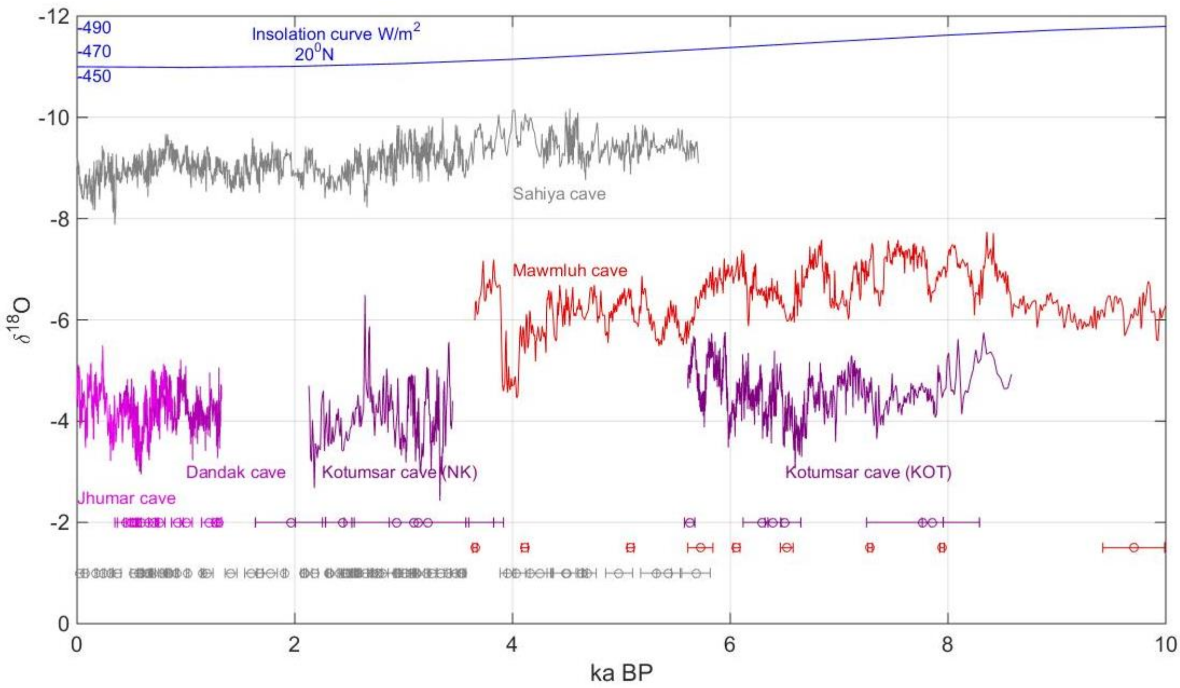

Figure 7. ISM stalagmite δ18O records on Holocene time scale. Sahiya [10,12], Mawmluh [45], Kotumsar (KOT-[57], NK-Supplementary Materials) , Dandak [9] and Jhumar [11] cave records have been shown along with their U-Th age errors. The insolation curve in W/m2 at 20°N has been shown in blue [105].

6. Future directions

Two decades of stalagmite δ18O based reconstructions of the ISM from India at the proximal end of the ISM, has shown that past variability of the ISM lies beyond the boundaries suggested by the short instrumental records. Solar insolation changes, dynamics in the North Atlantic region and Pacific Ocean SST's significantly drive the ISM on different time scales. Data-model comparisons of δ18O in climate states different from the present further re-enforce the strength of stalagmite δ18O based monsoon reconstructions. This in turn increases confidence in the ability of AGCM's to predict future changes in the ISM. The significant advances made in this field give us a better idea of fruitful future directions of research. Some of these are mentioned below:

1. The use of uranium-thorium dating methods coupled with the strong seasonality of the monsoon allow for high resolution records with high dating precision. This allows for precise age control on the timing of events and in turn gives significant insight into the pathway of distal forcings on the ISM. However, this requires consistency in age model creation which is a significant thrust area of the SISAL Working Group.
2. There is less information available on multi-decadal variability of the ISM and on the frequency of variability within different climate states. The age control provided by stalagmites coupled with high growth rates allows for more information on this variability through different methods of spectral analysis. This has been explored only to a limited extent in the current records and only to conclude with a range of plausible mechanisms. This area requires increased interaction between the paleoclimate and the atmospheric sciences community to narrow down the plausible physical mechanisms and pathways of forcings.
3. Databases such as SISAL, allow examination of regional patterns in records highlighting the sub-regional differences in responses of the ISM to forcings. At present, this is somewhat handicapped by the lack of long-term rainfall δ18O and cave monitoring studies. While δ18O gives information on large scale circulation changes, other stalagmite-based proxies like trace element ratios (such as Mg/Ca and U/Ca) can form powerful paleo-aridity indicators

Peer-reviewed version available at *Quaternary* **2018**, *1*, 29; doi:10.3390/quat1030029

providing information on local changes in rainfall. This not only provides information on local climate change but also on the sub-regional ISM response to distal forcings.

These steps should significantly improve the predictability of ISM variability which is the ultimate aim of such paleoclimate investigations.

Supplementary Materials: The following are available online at www.mdpi.com/xxx/s1, Kotumsar-NK record, Figure S4:-comparison of Valmiki cave records (VSPM1 and VSPM4).

Author Contributions: First draft of the paper was written by NK. SB drafted the abstract and has provided significant reviews and edits. FL has produced figure 5, edited figure 2, provided information on northeast Indian caves and climate and provided significant reviews and edits. Discussion with AS was useful in designing the structure of the paper. AS also provided information on north Indian climate and caves. VT provided information on north and northeast Indian geology and caves. MA provided information on deglacial $\delta^{18}O$ records from peninsular India. MB provided information on spectral analysis and reviews and edits. Shraddha Band provided information on peninsular Indian caves. GH provided useful feedback on the final draft of the paper. SB, MY and RR provided U-Th and $\delta^{18}O$ data of the published Kotumsar sample (KOT; Band et al., 2018). NK, GH, SB, MY and RR provided U-Th and $\delta^{18}O$ data of the unpublished Kotumsar sample (NK).

Funding: This research received no external funding.

Acknowledgments: SISAL (Speleothem Isotope Synthesis and Analysis) is a Working Group of PAGES (Past Global Changes) program. We thank PAGES for their support for this activity. We would also like to thank WoKAM (World Karst Aquifer Map) for providing the base karst map for the region. We further acknowledge Sahar Mozhdehi and Laia Comas-Bru for creating the code and generating Figure 2. The authors were greatly saddened by the death of Prof. Ramesh prior to this publication. He was instrumental in much of this work and will be greatly missed. The first author would also like to thank the speleothem group at Physical Research Laboratory for their support and cooperation with stalagmite work in India. And the speleothem group at the University of Oxford for their expertise and five wonderful and fruitful years of stalagmite research.

Conflicts of Interest: The authors declare no conflict of interest.

References

1. Webster, P. J.; Magaña, V. O.; Palmer, T. N.; Shukla, J.; Tomas, R. A.; Yanai, M.; Yasunari, T. Monsoons: Processes, predictability, and the prospects for prediction. *JGR: Oceans* **1998**, *103*, 14451–14510, doi:10.1029/97JC02719.
2. Mohtadi, M.; Prange, M.; Steinke, S. Palaeoclimatic insights into forcing and response of monsoon rainfall. *Nature* **2016**, *533*, 191–199, doi:10.1038/nature17450.
3. Li, H.-C.; Ku, T.-L.; You, C.-F.; Cheng, H.; Edwards, R. L.; Ma, Z.-B.; Tsai, W.; Li, M.-D. 87Sr/86Sr and Sr/Ca in speleothems for paleoclimate reconstruction in Central China between 70 and 280 kyr ago. *GCA* **2005**, *69*, 3933–3947, doi:10.1016/j.gca.2005.01.009.
4. Johnson, K. R.; Hu, C.; Belshaw, N. S.; Henderson, G. M. Seasonal trace-element and stable-isotope variations in a Chinese speleothem: The potential for high-resolution paleomonsoon reconstruction. *EPSL* **2006**, *244*, 394–407, doi:10.1016/j.epsl.2006.01.064.
5. Cheng, H.; Sinha, A.; Wang, X.; Cruz, F. W.; Edwards, R. L. The Global Paleomonsoon as seen through speleothem records from Asia and the Americas. *Clim Dyn* **2012**, *39*, 1045–1062, doi:10.1007/s00382-012-1363-7.
6. Wang, Y. J.; Cheng, H.; Edwards, R. L.; An, Z. S.; Wu, J. Y.; Shen, C.-C.; Dorale, J. A. A High-Resolution Absolute-Dated Late Pleistocene Monsoon Record from Hulu Cave, China. *Science* **2001**, *294*, 2345–2348, doi:10.1126/science.1064618.
7. Wang, Y.; Cheng, H.; Edwards, R. L.; He, Y.; Kong, X.; An, Z.; Wu, J.; Kelly, M. J.; Dykoski, C. A.; Li, X. The Holocene Asian Monsoon: Links to Solar Changes and North Atlantic Climate. *Science* **2005**, *308*, 854–857, doi:10.1126/science.1106296.

8. Wang, Y.; Cheng, H.; Edwards, R. L.; Kong, X.; Shao, X.; Chen, S.; Wu, J.; Jiang, X.; Wang, X.; An, Z. Millennial- and orbital-scale changes in the East Asian monsoon over the past 224,000 years. *Nature* **2008**, *451*, 1090–1093, doi:10.1038/nature06692.
9. Sinha, A.; Cannariato, K. G.; Stott, L. D.; Cheng, H.; Edwards, R. L.; Yadava, M. G.; Ramesh, R.; Singh, I. B. A 900-year (600 to 1500 A.D.) record of the Indian summer monsoon precipitation from the core monsoon zone of India. *GRL* **2007**, *34*, doi:10.1029/2007GL030431.
10. Sinha, A.; Kathayat, G.; Cheng, H.; Breitenbach, S. F. M.; Berkelhammer, M.; Mudelsee, M.; Biswas, J.; Edwards, R. L. Trends and oscillations in the Indian summer monsoon rainfall over the last two millennia. *Nature Comm.* **2015**, *6*, doi:10.1038/ncomms7309.
11. Sinha, A.; Berkelhammer, M.; Stott, L.; Mudelsee, M.; Cheng, H.; Biswas, J. The leading mode of Indian Summer Monsoon precipitation variability during the last millennium. *GRL* **2011**, *38*, doi:10.1029/2011GL047713.
12. Kathayat, G.; Cheng, H.; Sinha, A.; Yi, L.; Li, X.; Zhang, H.; Li, H.; Ning, Y.; Edwards, R. L. The Indian monsoon variability and civilization changes in the Indian subcontinent. *Science Advances* **2017**, *3*, e1701296, doi:10.1126/sciadv.1701296.
13. Kathayat, G.; Cheng, H.; Sinha, A.; Spötl, C.; Edwards, R. L.; Zhang, H.; Li, X.; Yi, L.; Ning, Y.; Cai, Y.; Lui, W. L.; Breitenbach, S. F. M. Indian monsoon variability on millennial-orbital timescales. *Scientific Reports* **2016**, *6*, doi:10.1038/srep24374.
14. Myers, C. G.; Oster, J. L.; Sharp, W. D.; Bennartz, R.; Kelley, N. P.; Covey, A. K.; Breitenbach, S. F. M. Northeast Indian stalagmite records Pacific decadal climate change: Implications for moisture transport and drought in India. *GRL* **2015**, *42*, 4124–4132, doi:10.1002/2015GL063826.
15. Sinha, A.; Cannariato, K. G.; Stott, L. D.; Li, H.-C.; You, C.-F.; Cheng, H.; Edwards, R. L.; Singh, I. B. Variability of Southwest Indian summer monsoon precipitation during the Bølling-Ållerød. *Geology* **2005**, *33*, 813–816, doi:10.1130/G21498.1.
16. Dutt, S.; Gupta, A. K.; Clemens, S. C.; Cheng, H.; Singh, R. K.; Kathayat, G.; Edwards, R. L. Abrupt changes in Indian summer monsoon strength during 33,800 to 5500 years B.P. *GRL* **2015**, *42*, 5526–5532, doi:10.1002/2015GL064015.
17. Lechleitner, F. A.; Breitenbach, S. F. M.; Cheng, H.; Plessen, B.; Rehfeld, K.; Goswami, B.; Marwan, N.; Eroglu, D.; Adkins, J.; Haug, G. Climatic and in-cave influences on δ18O and δ13C in a stalagmite from northeastern India through the last deglaciation. *Quat. Res.* **2017**, *88*, 458–471, doi:10.1017/qua.2017.72.
18. LeGrande, A. N.; Schmidt, G. A. Sources of Holocene variability of oxygen isotopes in paleoclimate archives. *Clim. Past* **2009**, *5*, 441–455, doi:10.5194/cp-5-441-2009.
19. Battisti, D. S.; Ding, Q.; Roe, G. H. Coherent pan-Asian climatic and isotopic response to orbital forcing of tropical insolation. *JGR: Atmospheres* **2014**, *119*, 11,997-12,020, doi:10.1002/2014JD021960.
20. Atsawawaranunt, K.; Comas-Bru, L.; Amirnezhad Mozhdehi, S.; Deininger, M.; Harrison, S. P.; Baker, A.; Boyd, M.; Kaushal, N.; Ahmad, S. M.; Ait Brahim, Y.; Arienzo, M.; Bajo, P.; Braun, K.; Burstyn, Y.; Chawchai, S.; Duan, W.; Hatvani, I. G.; Hu, J.; Kern, Z.; Labuhn, I.; Lachniet, M.; Lechleiter, F. A.; Lorrey, A.; Pérez-Mejías, C.; Pickering, R.; Scroxton, N.; SISAL Working Group Members The SISAL database: a global resource to document oxygen and

carbon isotope records from speleothems. *Earth System Science Data Discussions* **2018**, 1–64, doi:https://doi.org/10.5194/essd-2018-17.

21. Dimri, A. P.; Niyogi, D.; Barros, A. P.; Ridley, J.; Mohanty, U. C.; Yasunari, T.; Sikka, D. R. Western Disturbances: A review. *Reviews of Geophys.* **2015**, *53*, 225–246, doi:10.1002/2014RG000460.
22. Breitenbach, S. F. M.; Adkins, J. F.; Meyer, H.; Marwan, N.; Kumar, K. K.; Haug, G. H. Strong influence of water vapor source dynamics on stable isotopes in precipitation observed in Southern Meghalaya, NE India. *EPSL* **2010**, *292*, 212–220, doi:10.1016/j.epsl.2010.01.038.
23. Murata, F.; Hayashi, T.; Matsumoto, J.; Asada, H. Rainfall on the Meghalaya plateau in northeastern India—one of the rainiest places in the world. *Nat Hazards* **2007**, *42*, 391–399, doi:10.1007/s11069-006-9084-z.
24. Kumar, K. K.; Soman, M. K.; Kumar, K. R. Seasonal forecasting of Indian summer monsoon rainfall: A review. *Weather 50*, 449–467, doi:10.1002/j.1477-8696.1995.tb06071.x.
25. Shukla, R. P.; Tripathi, K. C.; Pandey, A. C.; Das, I. M. L. Prediction of Indian summer monsoon rainfall using Niño indices: A neural network approach. *Atm. Res.* **2011**, *102*, 99–109, doi:10.1016/j.atmosres.2011.06.013.
26. Kumar, K. K. On the Weakening Relationship Between the Indian Monsoon and ENSO. *Science* **1999**, *284*, 2156–2159, doi:10.1126/science.284.5423.2156.
27. Ashok, K.; Guan, Z.; Yamagata, T. Impact of the Indian Ocean dipole on the relationship between the Indian monsoon rainfall and ENSO. *GRL* **2001**, *28*, 4499–4502, doi:10.1029/2001GL013294.
28. Kumar, P.; Kumar, K. R.; Rajeevan, M.; Sahai, A. K. On the recent strengthening of the relationship between ENSO and northeast monsoon rainfall over South Asia. *Clim Dyn* **2007**, *28*, 649–660, doi:10.1007/s00382-006-0210-0.
29. Ashok, K.; Yamagata, T. Climate change: The El Niño with a difference. *Nature* **2009**, *461*, 481–484, doi:10.1038/461481a.
30. Blanford, H. F. II. On the connexion of the Himalaya snowfall with dry winds and seasons of drought in India. *Proc. R. Soc. Lond.* **1884**, *37*, 3–22, doi:10.1098/rspl.1884.0003.
31. Hahn, D. G.; Shukla, J. An Apparent Relationship between Eurasian Snow Cover and Indian Monsoon Rainfall. *J. Atmos. Sci.* **1976**, *33*, 2461–2462, doi:10.1175/1520-0469(1976)033<2461:AARBES>2.0.CO;2.
32. Khandekar, M. L. Eurasian snow cover, Indian monsoon and El Niño/Southern Oscillation – a synthesis. *Atmosphere-Ocean* **1991**, *29*, 636–647, doi:10.1080/07055900.1991.9649422.
33. Kripalani, R. H.; Singh, S. V.; Vernekar, A. D.; Thapliyal, V. Empiriacal Study on Nimbus-7 Snow Mass and Indian Summer Monsoon Rainfall. *Int. Journ. of Climatology* **1996**, *16*, 23–34, doi:10.1002/(SICI)1097-0088(199601)16:1<23::AID-JOC988>3.0.CO;2-J.
34. Bamzai, A. S.; Shukla, J. Relation between Eurasian Snow Cover, Snow Depth, and the Indian Summer Monsoon: An Observational Study. *J. Climate* **1999**, *12*, 3117–3132, doi:10.1175/1520-0442(1999)012<3117:RBESCS>2.0.CO;2.
35. Kripalani, R.; Kulkarni, A. Climate impact of El Nino/La Nina on the Indian monsoon: A new perspective. *Weather* **2012**, doi:10.1002/j.1477-8696.1997.tb06267.x.

36. Goswami, B. N.; Mohan, R. S. A. Intraseasonal Oscillations and Interannual Variability of the Indian Summer Monsoon. *J. Climate* **2001**, *14*, 1180–1198, doi:10.1175/1520-0442(2001)014<1180:IOAIVO>2.0.CO;2.
37. Guhathakurta, P.; Rajeevan, M. Trends in the rainfall pattern over India. *Int. Journ. of Climatology* **2008**, *28*, 1453–1469, doi:10.1002/joc.1640.
38. Rajeevan, M.; Gadgil, S.; Bhate, J. Active and break spells of the Indian summer monsoon. *J Earth Syst Sci* **2010**, *119*, 229–247, doi:10.1007/s12040-010-0019-4.
39. Annamalai, H.; Slingo, J. M. Active / break cycles: diagnosis of the intraseasonal variability of the Asian Summer Monsoon. *Clim. Dyn.* **2001**, *18*, 85–102, doi:10.1007/s003820100161.
40. Mehta, V. M.; Lau, K.-M. Influence of solar irradiance on the Indian Monsoon-ENSO relationship at decadal-multidecadal time scales. *GRL* **1997**, *24*, 159–162, doi:10.1029/96GL03778.
41. Krishnan, R.; Sugi, M. Pacific decadal oscillation and variability of the Indian summer monsoon rainfall. *Clim. Dyn.* **2003**, *21*, 233–242, doi:10.1007/s00382-003-0330-8.
42. Chen, Z.; Auler, A. S.; Bakalowicz, M.; Drew, D.; Griger, F.; Hartmann, J.; Jiang, G.; Moosdorf, N.; Richts, A.; Stevanovic, Z.; Veni, G.; Goldscheider, N. The World Karst Aquifer Mapping project: concept, mapping procedure and map of Europe. *Hydrogeol J* **2017**, *25*, 771–785, doi:10.1007/s10040-016-1519-3.
43. Berkelhammer, M.; Sinha, A.; Mudelsee, M.; Cheng, H.; Edwards, R. L.; Cannariato, K. Persistent multidecadal power of the Indian Summer Monsoon. *EPSL* **2010**, *290*, 166–172, doi:10.1016/j.epsl.2009.12.017.
44. Singh Kotlia, B.; Singh, A. K. Stalagmite Inferred High Resolution Climatic Changes through Pleistocene-Holocene Transition in Northwest Indian Himalaya. *Journ. of Earth Sci. & Clim. Change* **2016**, *07*, doi:10.4172/2157-7617.1000338.
45. Berkelhammer, M.; Sinha, A.; Stott, L.; Cheng, H.; Pausata, F. S. R.; Yoshimura, K. An Abrupt Shift in the Indian Monsoon 4000 Years Ago. In *Geophysical Monograph Series*; Giosan, L., Fuller, D. Q., Nicoll, K., Flad, R. K., Clift, P. D., Eds.; American Geophysical Union: Washington, D. C., 2013; pp. 75–88 ISBN 978-1-118-70432-5.
46. Huguet, C.; Routh, J.; Fietz, S.; Lone, M. A.; Kalpana, M. S.; Ghosh, P.; Mangini, A.; Kumar, V.; Rangarajan, R. Temperature and Monsoon Tango in a Tropical Stalagmite: Last Glacial-Interglacial Climate Dynamics. *Scientific Reports* **2018**, *8*, 5386, doi:10.1038/s41598-018-23606-w.
47. Genty, D. Munagamanu cave data. SISAL database v1.
48. Joshi, L. M.; Kotlia, B. S.; Ahmad, S. M.; Wu, C.-C.; Sanwal, J.; Raza, W.; Singh, A. K.; Shen, C.-C.; Long, T.; Sharma, A. K. Reconstruction of Indian monsoon precipitation variability between 4.0 and 1.6 ka BP using speleothem δ<Superscript>18</Superscript>O records from the Central Lesser Himalaya, India. *Arab J Geosci* **2017**, *10*, 356, doi:10.1007/s12517-017-3141-7.
49. Raza, W.; Ahmad, S. M.; Lone, M. A.; Shen, C.-C.; Sarma, D. S.; Kumar, A. Indian summer monsoon variability in southern India during the last deglaciation: Evidence from a high resolution stalagmite δ18O record. *Palaeogeog., Palaeoclim., Palaeoeco.* **2017**, *485*, 476–485, doi:10.1016/j.palaeo.2017.07.003.

50. Lone, M. A.; Ahmad, S. M.; Dung, N. C.; Shen, C.-C.; Raza, W.; Kumar, A. Speleothem based 1000-year high resolution record of Indian monsoon variability during the last deglaciation. *Palaeogeog., Palaeoclim., Palaeoeco.* **2014**, *395*, 1–8, doi:10.1016/j.palaeo.2013.12.010.
51. Yadava, M. G.; Ramesh, R.; Pant, G. B. Past monsoon rainfall variations in peninsular India recorded in a 331-year-old speleothem. *The Holocene* **2004**, *14*, 517–524, doi:10.1191/0959683604hl728rp.
52. Laskar, A. H.; Raghav, S.; Yadava, M. G.; Jani, R. A.; Narayana, A. C.; Ramesh, R. Potential of Stable Carbon and Oxygen Isotope Variations of Speleothems from Andaman Islands, India, for Paleomonsoon Reconstruction. *JGR* **2011**, doi:10.1155/2011/272971.
53. Laskar, A. H.; Yadava, M. G.; Ramesh, R.; Polyak, V. J.; Asmerom, Y. A 4 kyr stalagmite oxygen isotopic record of the past Indian Summer Monsoon in the Andaman Islands. *Geochem., Geophys., Geosys.* **2013**, doi:10.1002/ggge.20203.
54. Allu, N. C.; Tiwari, M.; Yadava, M. G.; Dung, N. C.; Shen, C.-C.; Belgaonkar, S. P.; Ramesh, R.; Laskar, A. H. Stalagmite δ18O variations in southern India reveal divergent trends of Indian Summer Monsoon and East Asian Summer Monsoon during the last interglacial. *Quat. Int.* **2015**, *371*, 191–196, doi:10.1016/j.quaint.2014.12.014.
55. Kotlia, B. S.; Singh, A. K.; Zhao, J.-X.; Duan, W.; Tan, M.; Sharma, A. K.; Raza, W. Stalagmite based high resolution precipitation variability for past four centuries in the Indian Central Himalaya: Chulerasim cave re-visited and data re-interpretation. *Quat. Int.* **2017**, *444*, 35–43, doi:10.1016/j.quaint.2016.04.007.
56. Sanwal, J.; Kotlia, B. S.; Rajendran, C.; Ahmad, S. M.; Rajendran, K.; Sandiford, M. Climatic variability in Central Indian Himalaya during the last ~1800 years: Evidence from a high resolution speleothem record. *Quat. Int.* **2013**, *304*, 183–192, doi:10.1016/j.quaint.2013.03.029.
57. Band, S.; Yadava, M. G.; Lone, M. A.; Shen, C.-C.; Sree, K.; Ramesh, R. High-resolution mid-Holocene Indian Summer Monsoon recorded in a stalagmite from the Kotumsar Cave, Central India. *Quat. Int.* **2018**, *479*, 19–24, doi:10.1016/j.quaint.2018.01.026.
58. Sinha, N.; Gandhi, N.; Chakraborty, S.; Krishnan, R.; Ramesh, R.; Yadava, M.; Datye, A. Past rainfall reconstruction using speleothem from Nakarallu cave, kadapa, Andhra Pradesh, India. In; 2016; Vol. 18, pp. EPSC2016-811.
59. Liang, F.; Brook, G. A.; Kotlia, B. S.; Railsback, L. B.; Hardt, B.; Cheng, H.; Edwards, R. L.; Kandasamy, S. Panigarh cave stalagmite evidence of climate change in the Indian Central Himalaya since AD 1256: Monsoon breaks and winter southern jet depressions. *Quat. Sci. Rev.* **2015**, *124*, 145–161, doi:10.1016/j.quascirev.2015.07.017.
60. Kotlia, B. S.; Singh, A. K.; Joshi, L. M.; Dhaila, B. S. Precipitation variability in the Indian Central Himalaya during last ca. 4,000 years inferred from a speleothem record: Impact of Indian Summer Monsoon (ISM) and Westerlies. *Quat. Int.* **2015**, *371*, 244–253, doi:10.1016/j.quaint.2014.10.066.
61. Breitenbach, S. Changes in Monsoonal Precipitation and Atmospheric Circulation During the Holocene Reconstructed from Stalagmites from Northeastern India. Submitted, University of Potsdam: Potsdam, Germany, 2010.
62. Gebauer, H. Resources on the Speleology of Meghalaya State, India. Part 7: Khaddum (East Jaintia Hills District). *Berliner Höhlenkundliche Berichte* **2017**, *67*.

63. Gebauer, H. Resources on the Speleology of Meghalaya State, India. Part 6: Lumshnong (East Jaintia Hills). *Berliner Höhlenkundliche Berichte* **2015**, *60*.
64. Gebauer, H. Resources on the Speleology of Meghalaya State, India. Part 5: Syndai, Nongtalang and Lakadong. *Berliner Höhlenkundliche Berichte* **2013**, *52*.
65. Gebauer, H. Resources on the Speleology of Meghalaya State, India. Part 4: East Khasi Hills. Section 1 + 2. *Berliner Höhlenkundliche Berichte (BHB)* **2012**, *Volume 47–48*.
66. Gebauer, H. (Editor) Resources on the Speleology of Meghalaya State, India. Part 3: West Khasi Hills. *Berliner Höhlenkundliche Berichte* **2011**, *42*.
67. Gebauer, H. Resources on the Speleology of Meghalaya State, India. Part 2: Garo Hills. *Berliner Höhlenkundliche Berichte* **2009**, *35*.
68. Gebauer, H. Resources on the Speleology of Meghalaya State, India. Part 1: Overview. *Berliner Höhlenkundliche Berichte* **2008**, *33*.
69. Gebauer, H. Resources on the Speleology of Himachal Pradesh (India). *Berliner Höhlenkundliche Berichte* **2006**, *21*.
70. Gebauer, H. Resources on the Speleology of Jammu & Kashmir State, India. *Berliner Höhlenkundliche Berichte* **2005**, *18*.
71. Breitenbach, S.; Gebauer, H. Resources on the Speleology of Uttarakhand State (formerly Uttaranchal), India. *Berliner Höhlenkundliche Berichte* **2013**, *50*.
72. Tewari, V. C. Speleothems from Uttarakhand and Meghalaya indicating Holocene Monsoon and Climate. **2011**, *3*, 87–104.
73. Tewari, V. C. Speleothems as Paleoclimate and Paleomonsoon Indicator : Evidences from NW Himalaya and the Shillong Plateau, NE India. In *Selected Topics in Earth System Science*; 2013; pp. 31–39.
74. Tewari, V. Himalayan Speleothems as Proxy for the Past Climatic Change and Paleomonsoon. In *Frontiers of Earth Science*; Scientific Publishers (India), 2015; pp. 243–250.
75. Baskar, S.; Baskar, R.; Tewari, V. C.; Thorseth, I. H.; Øvreås, L.; Lee, N. M.; Routh, J. Cave Geomicrobiology in India: Status and Prospects. In *STROMATOLITES: Interaction of Microbes with Sediments*; Cellular Origin, Life in Extreme Habitats and Astrobiology; Springer, Dordrecht, 2011; pp. 541–569 ISBN 978-94-007-0396-4.
76. Brooks, S.; Smart, C. *Caving in the Abode of the Clouds. The Caves and Karst of Meghalaya, North East India. Bristol Exploration Club and Orpheus Caving Club, Somerset and Derbyshire. 1995.*;
77. Harries, D. B.; Ware, F. J.; Fischer, C. W.; Biswas, J.; Kharpran-Daly, B. D. A Review of Biospeleology of Meghalaya, India. *National Speleological Society Bulletin* **2008**, 15.
78. Yadava, M. G.; Ramesh, R. Monsoon reconstruction from radiocarbon dated tropical Indian speleothems. *The Holocene* **2005**, *15*, 48–59, doi:10.1191/0959683605h1783rp.
79. Biswas, J. Kotumsar Cave biodiversity: a review of cavernicoles and their troglobiotic traits. *Biodivers Conserv* **2010**, *19*, 275, doi:10.1007/s10531-009-9710-7.
80. Biswas, J.; Shrotriya, S. Dandak: a mammalian dominated cave ecosystem of India. *Subterranean Biology* **2011**, *8*, 1–8, doi:10.3897/subtbiol.8.1224.
81. Dar, F. A.; Perrin, J.; Riotte, J.; Gebauer, H. D.; Narayana, A. C.; Shakeel, A. Karstification in the Cuddapah Sedimentary Basin, Southern India: Implications for Groundwater Resources. *Acta Carsologica* **2011**, *40*.

82. Blaauw, M.; Christen, J. A.; Mauquoy, D.; van der Plicht, J.; Bennett, K. D. Testing the timing of radiocarbon-dated events between proxy archives. *The Holocene* **2007**, *17*, 283–288, doi:10.1177/0959683607075857.

83. Ramsey, C. B. Deposition models for chronological records. *QSR* **2008**, *27*, 42–60, doi:10.1016/j.quascirev.2007.01.019.

84. Scholz, D.; Hoffmann, D. L. StalAge – An algorithm designed for construction of speleothem age models. *Quat. Geochron.* **2011**, *6*, 369–382, doi:10.1016/j.quageo.2011.02.002.

85. Breitenbach, S. F. M.; Rehfeld, K.; Goswami, B.; Baldini, J. U. L.; Ridley, H. E.; Kennett, D. J.; Prufer, K. M.; Aquino, V. V.; Asmerom, Y.; Polyak, V. J.; Cheng, H.; Kurths, J.; Marwan, N. COnstructing Proxy Records from Age models (COPRA). *Clim. of the Past* **2012**, *8*, 1765–1779, doi:10.5194/cp-8-1765-2012.

86. Kim, S.-T.; Mucci, A.; Taylor, B. E. Phosphoric acid fractionation factors for calcite and aragonite between 25 and 75 °C: Revisited. *Chem. Geol.* **2007**, *246*, 135–146, doi:10.1016/j.chemgeo.2007.08.005.

87. Lachniet, M. S. Are aragonite stalagmites reliable paleoclimate proxies? Tests for oxygen isotope time-series replication and equilibrium. *GSA Bulletin* **2015**, *127*, 1521–1533, doi:10.1130/B31161.1.

88. Breitenbach, S. F. M.; Lechleitner, F. A.; Meyer, H.; Diengdoh, G.; Mattey, D.; Marwan, N. Cave ventilation and rainfall signals in dripwater in a monsoonal setting – a monitoring study from NE India. *Chem. Geol.* **2015**, *402*, 111–124, doi:10.1016/j.chemgeo.2015.03.011.

89. Lamb, H. H. The early medieval warm epoch and its sequel. *Palaeogeog., Palaeoclim., Palaeoeco.* **1965**, *1*, 13–37, doi:10.1016/0031-0182(65)90004-0.

90. Consortium, P. 2k; Ahmed, M.; Anchukaitis, K. J.; Asrat, A.; Borgaonkar, H. P.; Braida, M.; Buckley, B. M.; Büntgen, U.; Chase, B. M.; Christie, D. A.; Cook, E. R.; Curran, M. A. J.; Diaz, H. F.; Esper, J.; Fan, Z.-X.; Gaire, N. P.; Ge, Q.; Gergis, J.; González-Rouco, J. F.; Goosse, H.; Grab, S. W.; Graham, N.; Graham, R.; Grosjean, M.; Hanhijärvi, S. T.; Kaufman, D. S.; Kiefer, T.; Kimura, K.; Korhola, A. A.; Krusic, P. J.; Lara, A.; Lézine, A.-M.; Ljungqvist, F. C.; Lorrey, A. M.; Luterbacher, J.; Masson-Delmotte, V.; McCarroll, D.; McConnell, J. R.; McKay, N. P.; Morales, M. S.; Moy, A. D.; Mulvaney, R.; Mundo, I. A.; Nakatsuka, T.; Nash, D. J.; Neukom, R.; Nicholson, S. E.; Oerter, H.; Palmer, J. G.; Phipps, S. J.; Prieto, M. R.; Rivera, A.; Sano, M.; Severi, M.; Shanahan, T. M.; Shao, X.; Shi, F.; Sigl, M.; Smerdon, J. E.; Solomina, O. N.; Steig, E. J.; Stenni, B.; Thamban, M.; Trouet, V.; Turney, C. S. M.; Umer, M.; Ommen, T. van; Verschuren, D.; Viau, A. E.; Villalba, R.; Vinther, B. M.; Gunten, L. von; Wagner, S.; Wahl, E. R.; Wanner, H.; Werner, J. P.; White, J. W. C.; Yasue, K.; Zorita, E. Continental-scale temperature variability during the past two millennia. *Nature Geoscience* **2013**, *6*, 339–346, doi:10.1038/ngeo1797.

91. Cheng, H.; Edwards, R. L.; Broecker, W. S.; Denton, G. H.; Kong, X.; Wang, Y.; Zhang, R.; Wang, X. Ice Age Terminations. *Science* **2009**, *326*, 248–252, doi:10.1126/science.1177840.

92. Yoshimura, K.; Kanamitsu, M.; Noone, D.; Oki, T. Historical isotope simulation using Reanalysis atmospheric data. *JGR: Atmospheres* **2008**, *113*, doi:10.1029/2008JD010074.

93. Atwood, A. R.; Wu, E.; Frierson, D. M. W.; Battisti, D. S.; Sachs, J. P. Quantifying Climate Forcings and Feedbacks over the Last Millennium in the CMIP5–PMIP3 Models. *J. Climate* **2015**, *29*, 1161–1178, doi:10.1175/JCLI-D-15-0063.1.

Peer-reviewed version available at *Quaternary* **2018**, *1*, 29; doi:10.3390/quat1030029

94. Bond, G.; Kromer, B.; Beer, J.; Muscheler, R.; Evans, M. N.; Showers, W.; Hoffmann, S.; Lotti-Bond, R.; Hajdas, I.; Bonani, G. Persistent Solar Influence on North Atlantic Climate During the Holocene. *Science* **2001**, *294*, 2130–2136, doi:10.1126/science.1065680.
95. Rehfeld, K.; Marwan, N.; Breitenbach, S. F. M.; Kurths, J. Late Holocene Asian summer monsoon dynamics from small but complex networks of paleoclimate data. *Clim Dyn* **2013**, *41*, 3–19, doi:10.1007/s00382-012-1448-3.
96. Chen, J.; Chen, F.; Feng, S.; Huang, W.; Liu, J.; Zhou, A. Hydroclimatic changes in China and surroundings during the Medieval Climate Anomaly and Little Ice Age: spatial patterns and possible mechanisms. *QSR* **2015**, *107*, 98–111, doi:10.1016/j.quascirev.2014.10.012.
97. Dixit, Y.; Tandon, S. K. Hydroclimatic variability on the Indian subcontinent in the past millennium: Review and assessment. *Earth-Sci. Rev.* **2016**, *161*, 1–15, doi:10.1016/j.earscirev.2016.08.001.
98. Hartmut Schulz; Ulrich von Rad; Helmut Erlenkeuser; Ulrich von Rad Correlation between Arabian Sea and Greenland climate oscillations of the past 110,000 years. *Nature* **1998**, *393*, 54–57, doi:10.1038/31750.
99. Altabet, M. A.; Higginson, M. J.; Murray, D. W. The effect of millennial-scale changes in Arabian Sea denitrification on atmospheric CO_2. *Nature* **2002**, *415*, 159–162, doi:10.1038/415159a.
100. Ivanochko, T. S. Sub-Orbital Scale variations in the Intensity of the Arabian Sea Monsoon. *Edinburgh Research Archive* **2005**.
101. McGee, D.; Moreno-Chamarro, E.; Green, B.; Marshall, J.; Galbraith, E.; Bradtmiller, L. Hemispherically asymmetric trade wind changes as signatures of past ITCZ shifts. *QSR* **2018**, *180*, 214–228, doi:10.1016/j.quascirev.2017.11.020.
102. Pausata, F. S. R.; Battisti, D. S.; Nisancioglu, K. H.; Bitz, C. M. Chinese stalagmite $\delta^{18}O$ controlled by changes in the Indian monsoon during a simulated Heinrich event. *Nature Geoscience* **2011**, *4*, 474–480, doi:10.1038/ngeo1169.
103. Hemming, S. R. Heinrich events: Massive late Pleistocene detritus layers of the North Atlantic and their global climate imprint. *Reviews of Geophysics* **2004**, *42*, doi:10.1029/2003RG000128.
104. Stuiver, M.; Grootes, P. M.; Braziunas, T. F. The GISP2 δ18O Climate Record of the Past 16,500 Years and the Role of the Sun, Ocean, and Volcanoes. *Quaternary Research* **1995**, *44*, 341–354, doi:10.1006/qres.1995.1079.
105. Laskar, J.; Robutel, P.; Joutel, F.; Gastineau, M.; Correia, A. C. M.; Levrard, B. A long-term numerical solution for the insolation quantities of the Earth. *A&A* **2004**, *428*, 261–285, doi:10.1051/0004-6361:20041335.